Demyelination of superficial white matter in early Alzheimer's disease: a magnetization transfer imaging study

Eleonora Fornari[a,b,*], Philippe Maeder[a], Reto Meuli[a,b], Joseph Ghika[c],
Maria G. Knyazeva[a,c,*]

[a] Department of Radiology, Centre Hospitalier Universitaire Vaudois (CHUV) and University of Lausanne, Lausanne, Switzerland
[b] CIBM (Centre d'Imagérie Biomédicale), CHUV unit, Lausanne, Switzerland
[c] Department of Clinical Neuroscience, Centre Hospitalier Universitaire Vaudois (CHUV) and University of Lausanne, Lausanne, Switzerland

Abstract

Assuming selective vulnerability of short association U-fibers in early Alzheimer's disease (AD), we quantified demyelination of the surface white matter (dSWM) with magnetization transfer ratio (MTR) in 15 patients (Clinical Dementia Rating Scale [CDR] 0.5–1; Functional Assessment Staging [FAST]: 3–4) compared with 15 controls. MTRs were computed for 39 areas in each hemisphere. We found a bilateral MTR decrease in the temporal, cingulate, parietal, and prefrontal areas. With linear discriminant analysis, we successfully classified all the participants with 3 variates including the cuneus, parahippocampal, and superior temporal regions of the left hemisphere. The pattern of dSWM changed with the age of AD onset. In early onset patients, we found bilateral posterior demyelination spreading to the temporal areas in the left hemisphere. The late onset patients showed a distributed bilateral pattern with the temporal and cingulate areas strongly affected. A correlation with Mini Mental State Examination (MMSE), Lexis, and memory tests revealed the dSWM impact on cognition. A specific landscape of dSWM in early AD shows the potential of MTR imaging as an in vivo biomarker superior to currently used techniques.

© 2012 Elsevier Inc. All rights reserved.

Keywords: Alzheimer's disease; Demyelination; Magnetization transfer imaging; U-fibers

1. Introduction

Alzheimer's disease (AD) is an exclusively human disease, which prompts one to consider the human-specific features of brain organization as important risk factors. In comparison with other higher primates, which do not suffer from AD-like pathology, humans have significantly greater white matter (WM) volume (Bartzokis, 2004; Semendeferi et al., 2002). The myelin sheaths of axons facilitate the functions of a big size brain by speeding up and coordinating long distance signal transmission (Kimura and Itami, 2009) and by stabilizing the experience-dependent modifications of cortical networks (Fields, 2005). Hence the WM is an integral part of distributed cortical networks implementing memory, learning, and other cognitive functions affected by AD.

It has been noticed that AD progression inversely mirrors myelogenesis: the last areas to mature are the first to be damaged (Bartzokis, 2004; Braak and Braak, 1996; O'Sullivan et al., 2001; Stricker et al., 2009). In particular, conventional AD markers, beta-amyloid and tau protein fragments, are first found in the late-myelinating medial temporal and association cortices (Braak and Braak, 1996). Among the neuronal types, this pathology involves pyramidal neurons (Braak et al., 2006). Especially susceptible are

* Corresponding author at: Department of Radiology, CHUV, 1011 Lausanne, Switzerland. Tel.: +41 21 314 44 53; fax: +41 21 314 12 90.
E-mail address: Eleonora.Fornari@chuv.ch (E. Fornari).
* Alternate corresponding author at: Department of Neurology, CHUV, 1011 Lausanne, Switzerland. Tel.: +41 21 314 32 31; fax: +41 21 314 12 90.
E-mail address: Maria.Knyazeva@chuv.ch (M. Knyazeva).

pyramids in Layers III and V with protracted and incomplete myelination of their axons (Bussière et al., 2003; Morrison and Hof, 2007; Vogt et al., 1998). Such axons form the so-called association or U-fibers in the superficial white matter (SWM).

U-fibers leave the cortex and follow its folding within the underlying thin layer of the SWM. At a distance of up to 30 mm they re-enter the cortex, connecting adjacent gyri in this way (Schuz and Braitenberg, 2002). According to postmortem anatomical and in vivo magnetic resonance imaging (MRI)-based studies, U-fibers constitute the terminal zone of myelination and are incompletely myelinated until the third or fourth decade of life (Kinney et al., 1988; Parazzini et al., 2002; Yakovlev and Lecours, 1967). Therefore, in the cortical areas most vulnerable to AD, U-fibers seem to be the most vulnerable type of connections, yet, until now, these short association fibers have not been characterized in AD.

The MRI-based literature either considers the SWM together with the deep WM or only the latter compartment. Predominantly, magnetization transfer imaging (MTI) and diffusion weighted/tensor imaging (DWI/DTI) are used. The across-methods consensus is that the reduced WM integrity is typical for AD. In particular, the MTI studies reveal widespread WM damage (Bozzali et al., 2001; Van Es et al., 2007), especially prominent in the temporal lobe (Kabani et al., 2002; Van der Flier et al., 2002), while the DTI studies report damage throughout the deep WM structures including the posterior corpus callosum and the cingulum (Liu et al., 2009; Medina et al., 2006; Rose et al., 2008; Stahl et al., 2007; Stricker et al., 2009; for review see Thompson et al., 2007). The WM degradation is often correlated with cognitive decline (Huang and Auchus, 2007; Kavcic et al., 2008; Nakata et al., 2009).

We have chosen MTI for the SWM characterization. It estimates the efficiency of the magnetization exchange in biological tissues between a pool of free protons in intra- and extracellular water and a pool of protons bound to macromolecules. Because lipid bilayers strongly bind protons, the extent, concentration, and integrity of myelin membranes are the most important contributors to the magnetization transfer effect (Rovaris et al., 2003; Van Buchem et al., 1996; Van Waesberghe et al., 1998). In other words, MTI provides the myelin-based contrast independently from the spatial organization of white matter fibers. Being relatively short, the U-fibers allow the SWM mapping at a fine Brodmann-like scale. Considering that it is a typical spatial distribution of biomarkers rather than their specificity per se that points to the AD diagnosis, only an entire pattern of the SWM demyelination would serve as an in vivo marker of AD. Thus, for the SWM with its complex organization of fibers, MTI is the method of choice, because it does not depend upon fiber orientation and preserves accuracy throughout the whole brain.

We hypothesized that the SWM, predominantly composed of U-fibers, is selectively susceptible to the demyelination due to AD-related pathological processes. Furthermore, its damage should impact cognitive deterioration in AD patients. Imaging the SWM demyelination would provide an AD-specific spatial pattern at a fine scale sufficient for new insights into the role of demyelination in AD and for subsequent clinical applications.

2. Methods

2.1. Patients and control subjects

This study is based on the MTI data of 15 newly diagnosed AD patients from a larger sample in which the topography of functional cortical connectivity was studied (Knyazeva et al., 2010). The patients were recruited from the Memory Clinic of the Neurology Department, Centre Hospitalier Universitaire Vaudois (CHUV), Lausanne, Switzerland. Screening and assignment of diagnosis resulted from a multidisciplinary discussion of the cases between 2 senior neuropsychologists with 10 years of experience in a memory clinic, who tested both the patients and controls, a senior geriatrician, and a specialized Harvard Medical School trained senior neurologist (JG) with 25 years of experience in a memory clinic. To reach a diagnostic consensus, the team reviewed together all the clinical and radiological features. The severity and duration of disease were estimated from the heteroanamnesis provided by the caregiver. The Clinical Dementia Rating Scale (CDR) assessment form was filled out by the CDR certified senior neurologist (JG).

The AD group included 6 women and 9 men (Table 1). Fifteen control subjects (9 women and 6 men) were volunteers (mostly partners, caregivers, or family members of the

Table 1
Demographic and neuropsychologic characteristics of AD patients and control subjects

Characteristic	Patients	Control subjects	p
Number of subjects	15	15	
Gender	6 W/9 M	9 W/6 M	
Age	67.93 ± 10.55	64.47 ± 11.51	0.40
Education	11.33 ± 3.39	13.27 ± 3.43	0.15
MMSE	21.47 ± 4.03	28.87 ± 1.13	0.001
Disease duration (years)	4.4 ± 2.23	—	—
CDR	0.80 ± 0.25	—	—
FAST	3.93 ± 0.28	—	—
Mattis	112.64 ± 9.83	—	—
Mattis memory test	15.53 ± 4.27	—	—
Grober and Buschke test	8.45 ± 4.52	—	—
Baddeley's shape test	4.14 ± 3.86	—	—
Lexis	45.21 ± 9.65	—	—

The second and third columns present group characteristics, mean ± SD. The fourth column presents p values for the statistical significance of the between group differences estimated by Mann-Whitney Wilcoxon test.
Key: AD, Alzheimer's disease; CDR, Clinical Dementia Rating; FAST, Functional Assessment Staging; M, men; MMSE, Mini Mental State Examination; W, women.

patients). The patient and control groups differed neither in age nor in their level of education. All but 1 participant in both groups were right-handed. All the patients, caregivers, and control subjects gave written informed consent. All the applied procedures conform to the Declaration of Helsinki (1964) by the World Medical Association concerning human experimentation and were approved by the local Ethics Committee of Lausanne University.

The clinical diagnosis of probable AD was made according to the National Institute of Neurological and Communicative Disorders and Stroke and the Alzheimer's Disease and Related Disorders Association (NINCDS-ADRDA) criteria (McKhann et al., 1984), allowing a certainty of about 85% in the diagnosis. Cognitive functions were assessed with the Mini Mental State Examination (MMSE; Folstein et al., 1975) and with a detailed standardized neuropsychological assessment scale carried out by the Groupe de Réflexion sur les Evaluations Cognitives (GRECO) group for the French speaking population (Puel and Hugonot-Diener, 1996). To improve compatibility across studies, the stage of dementia was determined both according to the Functional Assessment Staging (FAST; Sclan and Reisberg, 1992) and to the Clinical Dementia Rating Scale (CDR; Morris, 1993). For this analysis we selected patients with mild dementia (FAST 3–4 and CDR 0.5–1). Additionally to the basic neuropsychological assessment, the severity of memory deficits considered to be typical early symptoms of AD was examined by means of the Mattis Dementia Rating Scale (Mattis, 1976). Episodic verbal memory was evaluated using the 16-item test by Grober and Buschke (Grober and Buschke, 1987). Episodic nonverbal memory was assessed through the shape test from the "Doors and People" test (Baddeley et al., 1994). Access to semantic knowledge was tested by means of naming pictures of a series of 64 pictures (Lexis test; DePartz et al., 2001).

Complete laboratory analyses and diagnostic neuroimaging (computerized tomography [CT] or MRI) were performed in order to rule out cognitive dysfunctions related to causes other than AD. In particular, the exclusion criteria were severe physical illness, psychiatric or neurological disorders associated with potential cognitive dysfunction, other dementia conditions (frontotemporal dementia, dementia associated with Parkinsonism, Lewy Body disease, pure vascular or prion dementia, etc.), alcohol/drug abuse, regular use of neuroleptics, antidepressants with anticholinergic action, benzodiazepines, stimulants, or β-blockers, and stages of AD beyond CDR 0.5–1.

We estimated the duration of the disease as the time in years between the onset of the recent episodic memory symptoms reported by the patient or relatives and the date of the neuropsychological examination, as recommended in the American Academy of Neurology (AAN) Practice Handbook (1994. Practice parameter for diagnosis and evaluation of dementia. (summary statement) Report of the Quality Standards Subcommittee of the American Academy

of Neurology. Neurology 44, 2203–2206). Control subjects underwent a brief clinical interview and the MMSE, to confirm the absence of cognitive deficits, of the use of psychoactive drugs, and of diseases that may interfere with cognitive functions. Only individuals with no cognitive complaints and a score ≥28 for a high and ≥26 for a low level of education were accepted as controls. All control subjects underwent a brain MRI.

2.2. MTI protocol

All patients and controls were scanned in a 3 Tesla Philips Achieva scanner (Philips, Best, the Netherlands). The protocol included a sagittal T1-weighted 3D gradient-echo sequence (magnetization-prepared rapid acquisition gradient echo [MPRAGE], 160 slices, 1 mm isotropic voxels) as a basis for segmentation. MTI was performed by running a gradient echo sequence (flip angle [FA] 20, time to echo [TE] 10, matrix size 192 × 192, pixel size 1.3 × 1.3 mm, 52 slices [thickness 2.5 mm]) twice, first with and then without a magnetization transfer (MT) saturation pulse. The MT weighting was obtained by using a radio frequency prepulse to partially saturate the immobile protons bound to macromolecules, which present a broad absorption spectrum compared with the free water protons. The saturation of the macromolecular protons indirectly causes a decrease of the magnetization of the mobile protons by magnetization transfer. When an on-resonance excitation pulse is applied after an off-resonance pulse, the received magnetic resonance (MR) signal is lower than without that prepulse. The myelin, consisting in a lipid bilayer, in which protons are embedded and surrounded by a limited extracellular space containing water and plasma derivatives, makes WM highly susceptible to the MT effect since the large number of macromolecular bound protons enables a high cross-relaxation rate with mobile water protons. We used a Gaussian MT prepulse with a duration of 7.68 ms, FA 500, and with a frequency offset of 1.5 kHz. The entire protocol lasted 22 minutes.

2.3. MTI metric

MT acquisitions were coregistered on the high resolution T1 acquisition. For every intracranial voxel (spatial resolution ~4 mm³), we calculated the magnetization transfer ratio (MTR) as follows:

$$MTR = (M_0 - M_s)/M_0 \times 100\%,$$

where M_S represents the intensity of the signal in a voxel with saturation, M_0 without saturation. The ratio indicates the percentage loss of signal intensity attributable to the MT effect. Because this effect is mainly dependent on myelin concentration (Stanisz et al., 1999), a decrease in MTR values is considered to be a sign of demyelination and/or a loss of axons. In this study we have chosen region of interest (ROI)-based mean MTR values as an estimator of demyelination. This parameter was preferred to the often used and

more sensitive MTR peak height or location because of the relatively fine scale of measurements required here by Brodmann-like mapping. We analyzed ROIs within the wide range between 364 and 6234 voxels, i.e., including quite small volumes. For minor volumes, significant variations of the peak height and position have been shown among and within subjects (Sormani et al., 2000). Therefore, by using the average MTR value, we sacrificed sensitivity for the sake of reliability of the results as is done in lesion studies with similar ROI volumes (Cercignani et al., 2001; Tjoa et al., 2008). In order to minimize the effect of noise, cerebral spinal fluid, and of partial volume (Bosma et al., 2000), only voxels with MTR >10% were included in the analysis. Image processing was performed using SPM8 (Wellcome Trust Centre for Neuroimaging, UCL Institute of Neurology, London, UK; http://www.fil.ion.ucl.ac.uk/spm/) and ad hoc routines developed in the MATLAB 7.1 environment (The MathWorks, Inc.; http://www.mathworks.in).

2.4. Segmentation of white and gray matter

For each subject, the high-resolution anatomical T1 images of the brain were segmented using a cluster analysis (SPM8) (Ashburner and Friston, 2000). The procedure is based on the between-voxel intensity differences and prior knowledge of the spatial distribution of tissues in the normal brain. The outcomes of this procedure are the probability maps of the gray matter (GM), of the WM, and of the

cerebrospinal fluid in the T1 native space, and parameters of the affine normalization procedure estimated to fit each subject's morphology to the Montreal Neurological Institute (MNI) template.

The selection of a target layer of WM for further analysis was performed in 3 steps (Fig. 1). First, from the WM probability map we identified the entire WM volume by thresholding the map at $p > 0.95$. The selected high level of significance allowed us to minimize the partial volume effect in the selected voxels. Second, the thus-defined WM mask was submitted to an iterative erosion process ending at a depth of 3 mm from the GM/WM boundary. Third, we selected subcortical WM by subtracting the eroded volume from the original WM mask (white contours in Fig. 1A). These steps were performed by in-house-made routines in Matlab language. Similarly, the mask for the GM was obtained by thresholding the corresponding probability map at $p > 0.95$.

2.5. Parcellation of hemispheres

Because the AD process inversely mirrors myelogenesis and because of the similarity between cytoarchitectonic and myelogenetic maps, the Brodmann's scale was an optimal choice for mapping demyelination. Each hemisphere was divided into 39 ROIs mainly corresponding to Brodmann areas (Table S1). They were automatically defined with a standard spatially normalized data set of anatomical land-
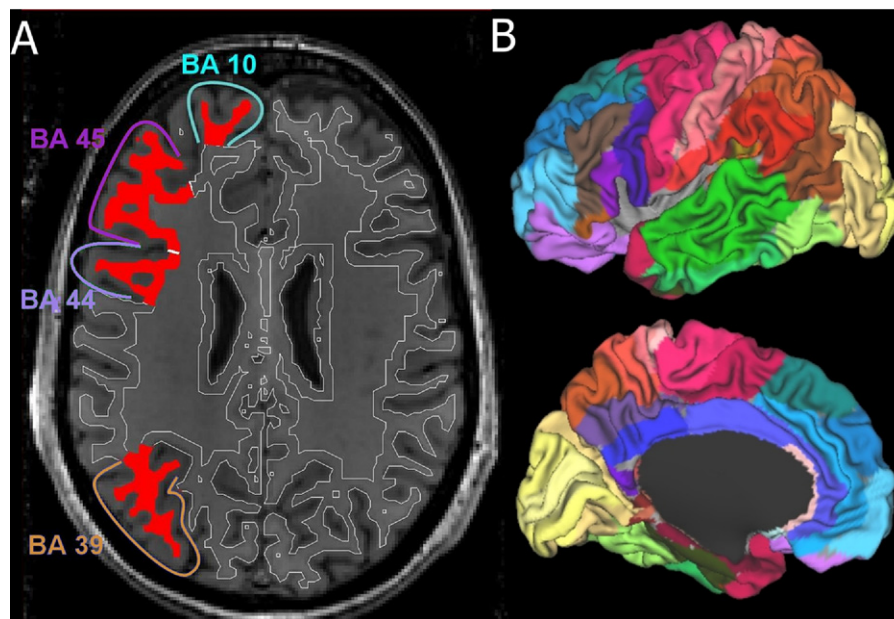

Fig. 1. Region of interest (ROI) selection and parcellation of hemisphere. In the left panel (A), the transversal slice at Z = 24 mm (according to the Montreal Neurological Institute [MNI] coordinate system) is shown. The external white contour represents the white matter (WM) mask as calculated when thresholding the WM probability map at $p > 0.95$. The internal white line represents the outcome of the erosion process of 3 mm in depth. The WM between these 2 lines was considered for parcellation into ROIs and for calculation of the mean magnetization transfer ratio (MTR) values. The selected cortical Brodmann areas (BAs) are shown in different colors together with their superficial white matter (SWM) ROIs in red. In the right panel (B), the representation of the final parcellation of the hemispheres is shown on a surface representing the boundary between gray matter (GM) and WM. Different BAs within each lobe are designated with different nuances of the same color.

marks using the Brodmann Atlas in the MNI space (WFU PickAtlas toolbox for SPM; ANSIR Laboratory, WFU School of Medicine Medical Center Winston-Salem, NC) (Maldjian et al., 2003). To adapt these ROIs to the single subject's morphology, they were exported to the subject's native space by inverting the normalization parameters obtained during the segmentation process. Then each ROI was submitted to a growth process in order to intersect the 3-mm-thick layer of the WM and applied to the coregistered MTR images. Each voxel of the WM layer was assigned to the closest ROI defined by the Brodmann areas (BAs). The quality of parcellation was visually inspected for each individual subject and statistically estimated for the group data. The distribution of the number of voxels across the ROIs (nonparametric Komogorov-Smirnov test, $p = 0.1$) as well as the mean number of voxels in each ROI (*t* test, $p > 0.3$) did not differ between the patients and controls. For statistical analysis we calculated the mean MTR value for each ROI of each subject.

2.6. Statistical analysis

Statistical analysis included, first, testing the differences between the ROI-based MTR mean values of patients and controls with a 2-sample *t* test, Bonferroni-corrected for the number of areas in each hemisphere at $p < 0.05$. For each ROI we also computed the effect size (d) by dividing the mean MTR difference between controls and patients by the common standard deviation of the 2 populations (Cohen, 1988). To link the individual MTI data to the clinical picture, we performed correlation analysis. In particular, patients' individual scores on MMSE, memory scales, and estimated duration of the disease served as predictors, and the regional MTR mean value as an outcome. We controlled the effect of age by introducing it as a nuisance variable in each correlation model. We considered the Pearson correlation coefficient (*r*) significant at $p < 0.01$.

The results of statistical analysis for 78 ROIs were exported into a 3D map defined by the MNI standard stereotaxic space (Fig. 1B). To display demyelination of each BA, we used a scale defined by the corresponding *t* values from statistical tests performed on the MTR values in the patients versus controls contrast or in the correlation analysis of the patient group. These results were displayed with the Caret software (brainmap.wustl.edu/caret) on a mesh representing the surface of GM-WM boundary of a standard MNI brain.

2.7. Linear discriminant analysis (LDA)

A logistic regression model was used to investigate the minimum number of regional mean MTR values sufficient to reliably discriminate patients from control subjects. Multivariate classification methods typically consist of 3 main stages: feature extraction, feature dimensionality reduction, and feature-based classification with cross-validation. Feature extraction was described in the previous paragraphs. To reduce the initial number of extracted features (39 BA areas ×

2 hemispheres), we used a variable ranking and a feed-forward selection procedure. The ranking step was defined by running a significant features test based on Fisher's criterion, a procedure that maximizes the separation between groups in a multidimensional feature-defined space using the ratio of the between-class variance to the within-class variance (Duda et al., 2001). It allowed us to rank the MTR values by optimizing the covariance matrix for subsequent feature classification based on the minimum number of significant features. The number of predictors included in the linear discriminant analysis (LDA) was then defined by including more and more variables starting from a single 1 with the highest loading and adding other variables in the order of decreasing loadings (stepwise feedforward procedure). The variable selection was stopped after the best discrimination power was achieved. The latter was defined as the percentage of correct classifications resulting from a leave-1-out validation procedure. It consists in iteratively removing 1 subject from the data set, constructing the predictor for the remaining data, and finally, classifying the removed subject.

3. Results

3.1. Regional MTR values: comparison between AD patients and controls

In AD patients, we found a widespread decrease in regional MTR values across the entire target volume excluding motor, premotor (BA 1–6), and right orbitofrontal (BA 11) areas (Fig. 2, Table S1). The most significant differences were found in the left hemisphere. They occurred in the parahippocampal (BA 27, 28, 35, 36) and the posterior cingulate, precuneus (BA 29–30), and cuneus regions. Similar MTR changes extended to the ventral cingulate area (BA 23), insula (BA 13, 43), the superior and middle temporal areas (BA 41, 42, 22, 37), and to Broca's area (BA 44, 45) (2-sample *t*-test, $p_{corrected} < 0.005$). The patients versus controls difference for the inferior temporal (BA 20, 38), prefrontal and frontal (BA 8, 9, 46), and visual extrastriate areas (BA 18, 19) was significant at $p_{corrected} < 0.01$. The symmetric regions in the right hemisphere showed a similar MTR pattern with a probability of a null hypothesis ranging between 0.01 and 0.05. The parietal (BA 7, 39, 40) and visual striate (BA 17) areas displayed a symmetrical decrease in both hemispheres at $p_{corrected} < 0.05$. The effect size measured by Cohen's *d* (Table S1) was large ($d > 1$) for as many as 29 and 25 areas, and medium ($0.76 < d < 0.99$) for 10 and 14 areas in the left and right hemisphere, respectively.

To address the issue of the neural basis of early versus late onset AD, we divided the whole group of newly diagnosed AD patients into subgroups according to their age (8 patients younger than 66 [60.1 ± 6.7], and 7 patients older than 70 years of age [76.8 ± 5.7]). The duration of the disease did not differ between these subgroups (4.9 ± 2.0
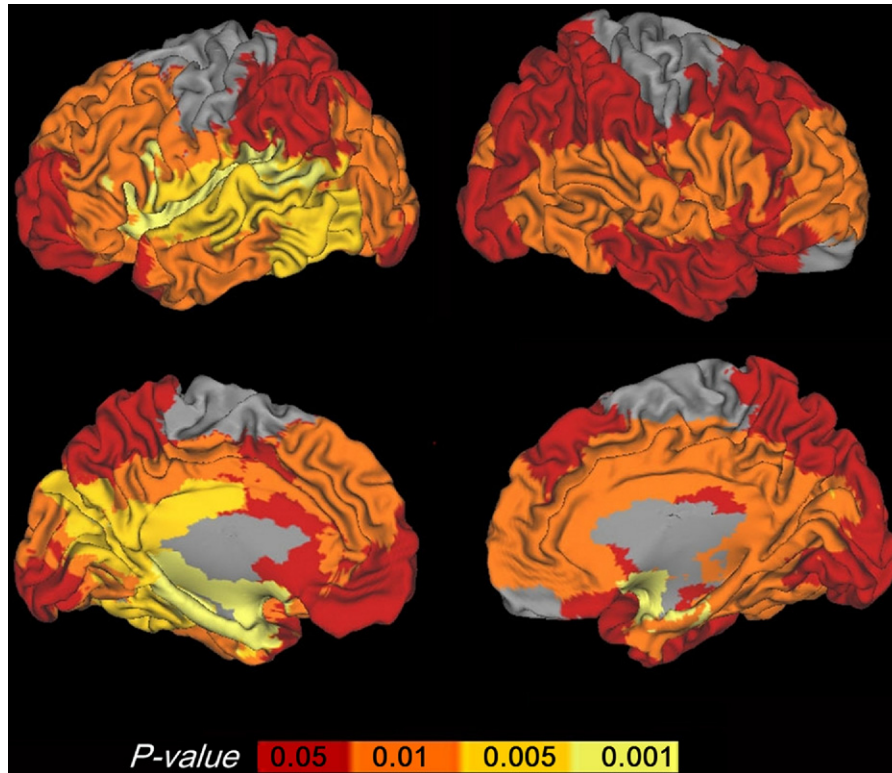
Fig. 2. Difference in regional myelination between Alzheimer's disease (AD) patients and elderly controls. The results of the 2-sample t test for mean magnetization transfer ratio (MTR) values are shown. Each region of interest (ROI) has been tested separately and the results are displayed in a 3D rendering. They are thresholded at $p < 0.05$ corrected for multiple comparisons. The color bar represents $p_{corrected}$ values. See Table S1 for details.

for early onset and 3.8 ± 2.5 for late onset). In comparison with controls, these subgroups showed clearly different patterns of SWM demyelination (Fig. 3). In particular, in early onset patients demyelinated areas ($p_{corrected} < 0.05$) mainly occupied posterior parts of the hemispheres including the bilateral occipital (BA 17, 18, 19), left cuneus and posterior cingulate (BA 23, 30), and inferior and posterior temporal (BA 21, 20, 37) areas. In addition, in the left hemisphere,

the reduced myelination extended anteriorly into the insular cortex (BA 13), the Rolandic operculum (BA 43), and Broca's area (BA 44).

The late onset patients showed a distributed pattern of areas with reduced MTR values ($p_{corrected} < 0.05$). These were the cuneus and cingulate (BA 23, 30, 31, 32), the superior temporal (BA 22), the insula (BA 13, 43), and frontal (BA 10, 44–45) regions bilaterally. They also in-
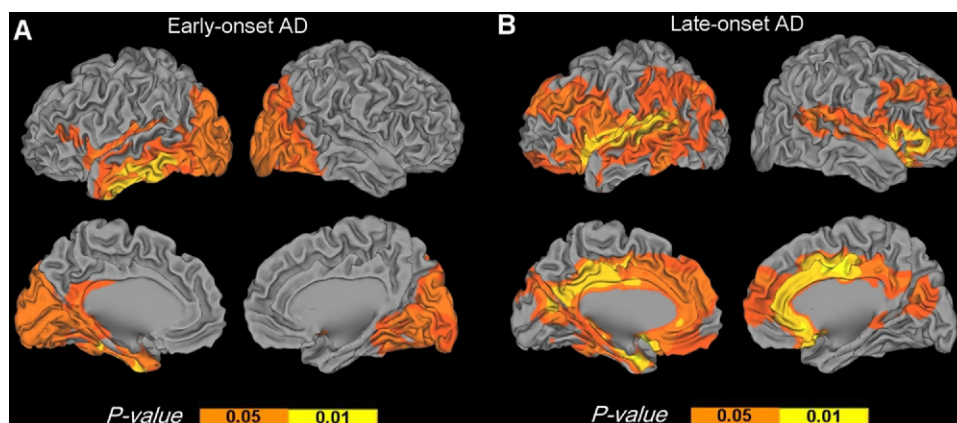

Fig. 3. Demyelination patterns in early- and late-onset Alzheimer's disease (AD). The results of the 2-sample t test ($p_{corrected} < 0.05$) are shown for the early-onset (left panel, A) and late-onset (right panel, B) patients.
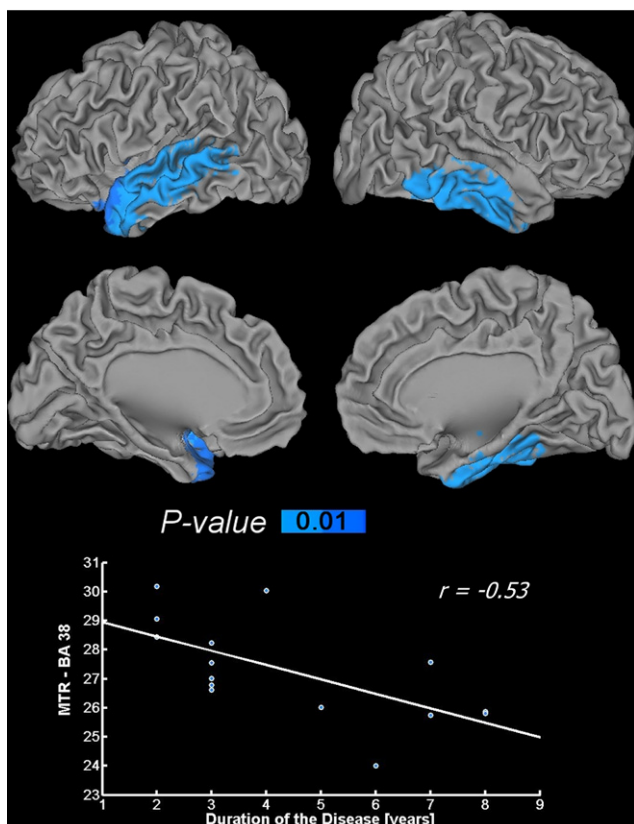
Fig. 4. Progression of superficial white matter (SWM) demyelination with duration of Alzheimer's disease (AD). The results of correlation analysis between regional magnetization transfer ratio (MTR) values and the estimated duration of the disease are depicted. Blue color bar represents p values for inverse Pearson's correlation coefficients at $p < 0.05$. The inverse correlation means that the longer the duration, the lower the SWM myelination in early AD. The scatter plot and regression line representing individual MTR values as a function of the duration of disease is presented for the Brodmann area (BA) 38 ($r = -0.53$).

cluded the orbitofrontal (BA 11), the posterior temporal (BA 37), and parietal lobule (BA 39–40) areas of the left hemisphere. Both subgroups demonstrated predominant involvement of the left hemisphere and, in particular, of the left temporal lobe. Moreover, for the whole AD group we found an inverse correlation between the duration of AD and MTR values in the superior (BA 22, 41–42) and middle (BA 21) temporal areas of the right hemisphere and in the inferior temporal areas (BA 20, 37) of the left hemisphere ($p < 0.01$, $-0.42 \geq r \geq -0.53$; Fig. 4). In other words, at the early stage, the AD progression correlates with the demyelination of SWM in the temporal lobe.

3.2. Linear discriminant analysis

We ran Fisher's ranking procedure for sorting the most explanatory features and reducing the dimensionality of the data separately for the 2 hemispheres (with 39 features in each 1) and then for the whole brain. In the left hemisphere, the cuneus (within BA 19), entorhinal (BA 28), and superior

temporal (BA 41) regions showed the highest loadings (4.73, 4.47, and 4.42, respectively). In the right hemisphere, the BA 28 and 34 (parahippocampal region) and cuneus turned out to be the best discriminating variables with loadings 4.29, 3.34, and 3.86, respectively. The feed-forward selection of features showing the highest discriminating loadings performed on the total number of areas gave the same results as for the left hemisphere alone (Fig. 5). The classification power increased from 66% (3 controls and 2 patients misclassified) with 1 input variable (left cuneus), to 80% (2 controls and 1 patient misclassified) with 2 inputs (left cuneus and parahippocampal region), and to a full discriminating power with 3 input variables (cuneus, parahippocampal region, and superior temporal region of the left hemisphere). The MTR abnormalities in AD patients were apparently asymmetric. However, the assessment of the interhemispheric asymmetry is outside of the scope of this report and will be presented elsewhere.

3.3. Regional MTR and the clinical picture in AD

To understand whether the demyelination of SWM contributes to cognitive impairment in AD, we considered the relationship between the state of mental health in AD patients and the severity of demyelination. To this end, first of all, we used a conventional metric for cognition — MMSE. In our AD group we found widespread territories, where MTR and MMSE scores directly correlated, i.e., the more the myelination of SWM was affected, the lower were the individual MMSE ratings (Fig. 6). As can be seen from the image, these areas include Broca's area (BA 44, 45), the bilateral insular region (BA 13, 43), the left superior temporal lobe (BA 41, 42) extending to the temporoparietal region (BA 39, 40), the cuneus (within BA 19), the cingulate sulcus (BA 23, 24, 31, 32), and primary visual areas (BA 17) bilaterally ($0.51 \leq r \leq 0.67$ at $p < 0.005$).

The scores on the Mattis memory scale that summarizes an entire set of different memory functions were associated with MTR values (Fig. S1) in the right hemisphere for the superior temporal (BA 22, 42) and frontal (BA 10, 45–47) cortices. For these areas, the Pearson's correlation coefficients (r) ranged between 0.41 (BA 10) and 0.47 (BA 45). Episodic visual memory scores (Doors and People Test, R1/12) also correlated with MTR values mainly in the left hemisphere (Fig. S2). The region, where individual scores were linked to SWM demyelination, included the parieto-temporal (BA 39, 40) and parahippocampal (BA 36) cortices. In the right hemisphere, correlations were limited to the insular cortex and prefrontal cortex (BA 46) at $p < 0.01$. Episodic verbal memory, examined with the Grober and Buschke test (T1/16), correlated with MTR scores (Fig. S3) predominantly in the left hemisphere, specifically in the superior parietal lobule (BA 5) and the parahippocampal area (BA 36). In the right hemisphere, only the superior parietal lobule (BA 5) turned out to be involved. The relationship between the naming ability estimated with the
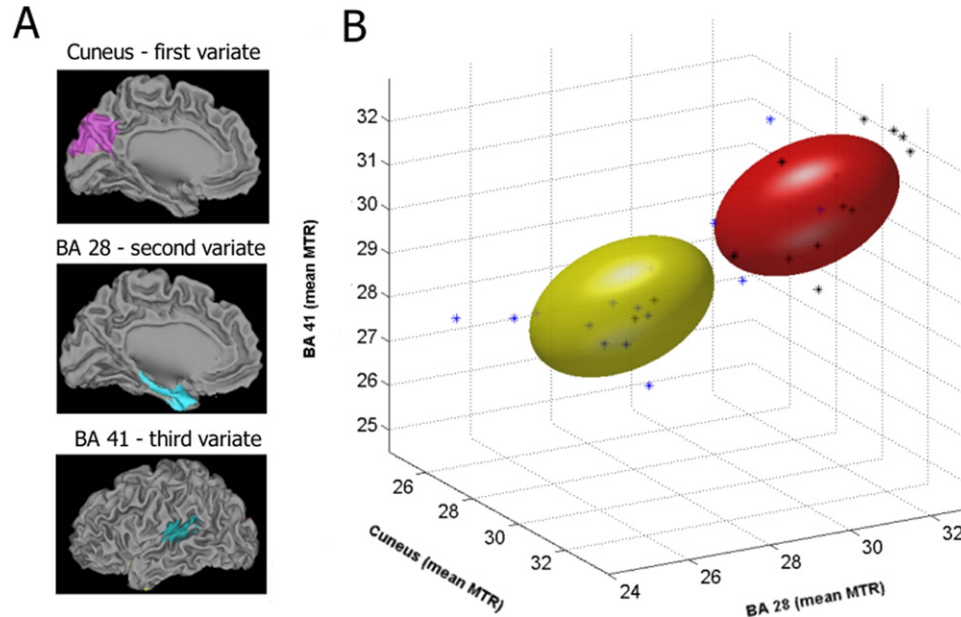
Fig. 5. Results of linear discriminant analysis. (A) The Alzheimer's disease (AD) patients were distinguished from controls without misclassifications by a linear combination of magnetization transfer ratio (MTR) values from cuneus (the first variate, in violet), Brodmann area (BA) 28 (the second variate, in blue), and BA 41 (the third variate, in green) of the left hemisphere. (B) The scatter plot shows the individual combinations of MTR values in the controls (black stars) and patients (blue stars). The ellipsoids represent the 95% confidence intervals for the patients (yellow) and controls (red). They are centered on the within-group means of the predictors. The image demonstrates a clear separation between the 2 groups (see the text for details).

Lexis test and demyelination was significant for the superior and middle temporal regions of the left hemisphere (BA 41, 42, 22) at $p < 0.01$ (Fig. S4).

4. Discussion

Here we report a widespread decrease of SWM myelination in early AD quantified with the MTI method. We found a specific landscape of demyelination characterized by the involvement of the cingulate, temporal, parietal, and frontal association areas. Although the demyelination was bilateral, the right hemisphere showed milder effects than the left hemisphere. Importantly, linear discriminant analysis achieved a full discriminating power — that is, correctly classified all the participants on the basis of only 3 variables: the superior temporal, parahippocampal, and cuneus regions of the left hemisphere. The pattern of demyelination depended on the age of AD onset. In early onset patients, we found bilateral posterior demyelination spreading to the temporal areas in the left hemisphere. The late onset patients showed a more distributed bilateral pattern with the temporal and cingulate regions strongly affected. A correlation with MMSE and various memory tests pointed to a significant impact of the SWM demyelination on the general mental state and on specific cognitive functions in AD patients.

4.1. Demyelination of U-fibers in AD

The superficial white matter has not been systematically studied in the elderly population or AD patients. To our knowledge, only 1 quantitative MRI report separately characterized the deep WM and the layer of U-fibers in normal middle-aged individuals (Wen and Sachdev, 2004). According to this study, the 4-mm-thick layer adjacent to the cortex is virtually free of lesions in contrast to the deep WM that shows widely dispersed lesions with the frontal and occipital lobes being most affected. This difference was accounted for by the pattern of vascularization of U-fibers, which are supplied by both deep and cortical arteries. A recently published DTI study of SWM predominantly characterized radially oriented fibers (Oishi et al., 2009). However, such fibers mostly represent long range association connections. They constitute only a small fraction of the SWM: the number of U-fibers is 2 orders of magnitude greater (Schuz and Braitenberg, 2002). Therefore, the impact of U-fibers on the SWM is expected to be overwhelming and requires a special analysis. Because the MTI does not depend upon the orientation of fibers within the SWM compartment, this method predominantly quantifies U-fibers.

Even a cursory examination of demyelination maps (Fig. 4) shows that the topography of SWM changes in AD is compatible with the distribution of amyloid plaques (Bartzokis et al., 2007; Buckner et al., 2005; Frisoni et al., 2009; Shin et al., 2008). However, in contrast with amyloid deposits, which are predominantly located in the convexity association cortex (Buckner et al., 2005; Frisoni et al., 2009), we have found the most pronounced SWM demyelination in the medial temporal areas, which makes its topog-
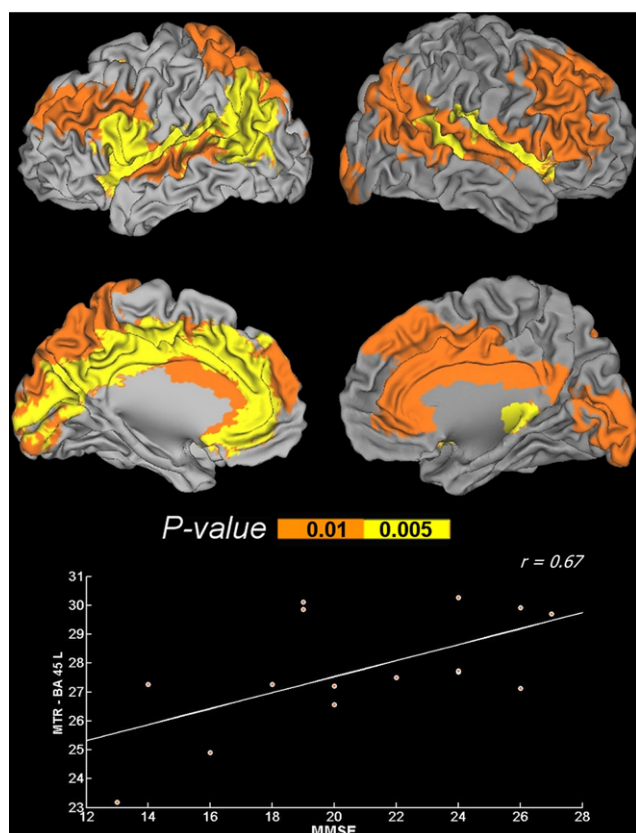
Fig. 6. Superficial white matter (SWM) demyelination correlates with general mental state in Alzheimer's disease (AD) patients. Correlation maps based on Pearson's correlation coefficients between individual Mini Mental State Examination (MMSE) scores and magnetization transfer ratio (MTR) values are shown. The color bar represents *p* values. The scatter plot and regression line show individual MTR values as a function of the MMSE score for the Brodmann area (BA) 41 in the left hemisphere ($r = 0.67$).

raphy more similar to that of neurofibrillary tangles and neuritic plaques (Nelson et al., 2009a; Shin et al., 2008).

The effect sizes (Table S1) suggest a certain temporal order of the AD-related SWM demyelination that starts in the medial temporal areas ($d_{mean} = 1.22$) and consequently spreads out to the association areas of the neocortex ($d_{mean} = 1.05$), sparing primary sensory-motor and orbitofrontal cortices at a relatively early (CDR 0.5–1) stage of the disease. This interpretation fits the known scenario, according to which AD begins in the entorhinal cortex, then spreads to the other medial temporal structures, and, finally, affects the convexity association cortices (Braak and Braak, 1996). It also agrees with the observation that the AD extension over the cortex inversely mirrors myelogenesis, as the temporal lobe, and, specifically, its basal and parahippocampal regions, have the most protracted cycle of myelination continuing into the fifth and even sixth decades of life (Bartzokis, 2004), yet the large effect sizes in the association cortex imply an early involvement of the convexital cortex in the pathological process.

Surprisingly, in our patients, the most affected areas also include the primary auditory area (BA 41) of the left hemisphere, which has the largest size effect. Moreover, together with the cuneus and parahippocampal regions, it perfectly discriminates AD patients from controls. In humans, the primary auditory areas are fully myelinated much later than the other primary areas (Yakovlev and Lecours, 1967). Their structural interhemispheric asymmetry is another important feature (Chance et al., 2006; Penhune et al., 1996). In the left hemisphere, the neuronal columns are wider and spaced further apart with the more myelinated connections between them (Seldon, 1981). Greater myelination and connectivity of the left primary auditory cortex are thought to underlie its specialization for speech processing (Seldon, 1981; Warrier et al., 2009). These very features might also increase the susceptibility of this area to AD, yet highly variable morphology of this region in the human brain (Penhune et al., 1996 Puel et al., 1996) calls for cautious interpretation and replication of the measurements.

The landscape of SWM demyelination appeared to be sensitive to the age of AD onset. In the early onset patients, the parieto-occipital SWM is affected, while in the late onset patients the damage is distributed across the temporal, frontal, and parietal areas, but the occipital ones are spared. The SWM of the medial cortex also reveals remarkable differences: the cingulate is spared in early- and strongly affected in late-onset AD. Although the data should be considered preliminary due to a small group size, such topography of demyelination in our early-onset patients is compatible with the so-called posterior variant of AD. The characteristic neuroimaging findings for visual AD involve bilateral posterior gray matter loss. The parietal, posterior cingulate, and precuneus regions are frequently among the affected cortices (Frisoni et al., 2007; Ishii et al., 2005; Schmidtke et al., 2005). The pattern of SWM demyelination found here in the old patients is close to the distribution of conventional AD biomarkers reported for late onset AD (Braak and Braak, 1996; Buckner et al., 2005; Frisoni et al., 2009; Shin et al., 2008).

In summary, the specific topography compatible with the distribution of the histochemical markers, high discriminative power, and sensitivity to the age of onset tightly link the demyelination of SWM to the AD pathological processes. Furthermore, the advanced level of demyelination in mild AD implies that the process emerges and develops for a long time in the prodromal phase and, therefore, might have a good prognostic potential for people with mild cognitive impairment or even for those without apparent cognitive problems.

4.2. Demyelination of U-fibers and cognitive decline in AD

An additional utility of the SWM demyelination evidence is provided by its association with cognitive decline in early AD. Indeed, despite being a hallmark of AD, neither

the burden of amyloid plaques (Duyckaerts et al., 2009) nor their removal (Holmes et al., 2008) correlates with cognitive performance in patients. Furthermore, although neurofibrillary (tau) pathology appears to be related to the severity of AD (for review see Duyckaerts et al., 2009; Nelson et al., 2009b), this relationship is reported for samples which include a wide range of cases (from mild to advanced) estimated on a relatively coarse scale (e.g., 5 levels of cognitive performance for the CDR). Such across-stage correlations acquire significance mainly due to the very high lesion counts in severely demented patients, implying low resolution of the marker in question at a fine scale limited to early stages of AD.

Recent reports show that the MR-based neuroimaging markers of the WM integrity in AD can successfully compete with the histochemical ones (Stebbins and Murphy, 2009). The DTI studies not only demonstrate that the changes in fiber integrity correlate with the AD progression to advanced stages (Nakata et al., 2009; Yoshiura et al., 2002), but also that links between some DTI metrics and cognitive decline are significant in the groups limited to mild AD. In particular, FA of the left cingulum was found to correlate with scores in verbal episodic memory, verbal recognition, and the Boston naming test in early AD (Fellgiebel et al., 2008). Another study (on mild AD patients) showed that posterior callosal FA correlates with verbal fluency and figural memory impairments, whereas posterior subcortical FA correlates with delayed verbal memory, figural memory, and optic flow perceptual impairments (Kavcic et al., 2008).

The SWM correlation maps are expected to reveal the "bottlenecks" emerging and developing due to AD in the distributed cortical networks underlying respective cognitive functions. Because with AD progression, abnormalities extend over the cortex in an orderly fashion, the topography of the affected regions that limit cognitive performance would vary at different AD stages. Hence, a correlation analysis of a roughly homogenous group (e.g., early AD) seems to be optimal for determining cortical modules that malfunction at a particular stage. In such a context, the MTI-based quantification of SWM demyelination holds substantial promise.

First of all, in our patients with mild AD (MMSE scores ranged between 13 and 27), a composite measure of cognitive status — MMSE — shows distributed correlations with the demyelination of the association neocortex that agree with the well established observation that the clinical symptoms of AD emerge together with the involvement of the convexity cortex (Morrison and Hof, 2007). The topography of these correlations clearly differentiates AD patients from elderly controls, in whom worsening in cognition is linked to the prefrontal areas (Gunning-Dixon et al., 2009; Madden et al., 2009) and fits the landscape of areas affected by AD (see above). Among the cerebral cognitive networks, those underlying memory functions are of special interest for this

discussion, because memory suffers first in AD. Strong correlations with the underlying neural substrate would suggest a method for their objective measurement, probably even before the emergence of neuropsychological symptoms.

Considering that the Mattis memory scale summarizes a set of memory tests and that involvement of the posterior areas is material-specific, whereas that of the prefrontal cortex is consistently demonstrated with diverse material across various recall/recognition paradigms (Duncan and Owen, 2000), we expected that the prefrontal cortex would be the most probable substrate for correlations. In fact, the correlation map for this scale revealed that memory decline is related to demyelination in the prefrontal and superior temporal territories of the right hemisphere. According to the hemispheric encoding/retrieval asymmetry hypothesis supported by neuroimaging results (Fletcher et al., 1998; Tulving et al., 1994), the left hemisphere implements the encoding, and the right hemisphere the retrieving of information. Therefore, our finding can be interpreted as a predominant impact of retrieval difficulties in early AD. Alternatively, it can be explained by compensatory strategies, due to which the less affected right hemisphere becomes involved in both encoding and retrieval. Previously, correlations between the verbal episodic memory dysfunction and glucose hypometabolism in the right parietotemporal and frontal cortices were also reported and interpreted as compensatory effects in AD (Desgranges et al., 1998b).

In line with the functional neuroimaging literature, the correlations for episodic memory tests would include material-specific correlations in the selected temporal, parietal, or occipital areas and consistent correlations in the parahippocampal cortex, a key component of the episodic memory system. Indeed, both episodic visual and episodic verbal memory scores correlated with SWM demyelination in the left parahippocampal cortex. In addition, the decline of episodic visual memory predictably correlated with the demyelination of the left parietotemporal cortex and of the right insular and prefrontal areas within the region usually activated by memory retrieval processes (covered by the Mattis memory scale correlations in this set of data). Interestingly, the episodic verbal memory decline appeared to be related to the SWM state of the superior parietal cortex that cannot be attributed to the material specificity. However, this region is frequently activated during episodic memory tasks. A recent hypothesis suggests that the dorsal parietal cortex allocates attentional resources to memory retrieval (Cabeza et al., 2008). In view of the strong involvement of this region in low confidence memory (Kim and Cabeza, 2009), its complementary role in episodic retrieval might be enhanced in AD, making the deterioration of this region critical for performance. Indeed, less activation during retrieval from episodic memory has been shown not only in the hippocampal, but also in the parietal cortex of AD

patients (Bäckman et al., 1999; Grön et al., 2002; Rémy et al., 2005).

Finally, the decline in the naming ability in our AD patients correlated with the demyelination of the left superior and middle temporal regions that is consistently found in functional activation studies within the extended cortical network of semantic memory (Cabeza and Nyberg, 2000). This is not surprising, given a strong relationship between naming ability and semantic knowledge. In AD, semantic memory dysfunction reliably correlates with the glucose hypometabolism in the temporal areas (Desgranges et al., 1998a; Hirono et al., 2001; Zahn et al., 2006). To summarize, both general cognitive decline and deterioration of particular memory functions in AD correlate with the demyelination of SWM within the neuroanatomic regions established for respective functions. Therefore, through the quantification of areal SWM, the MTI method can be used to assess regional pathology related to individuals' cognitive deficits in early AD.

The main limitation of our study arises from the small sample size that precludes immediate inferences regarding the clinical application of our findings and suggests the necessity for their validation with respect to a bigger cohort. The reliability of our findings would also benefit from a follow-up study linking the SWM demyelination to the clinical picture in individual patients. Although the clinical application of SWM analysis is of obvious interest, it will further require the adaptation of the computational demands to the clinical environment.

Disclosure statement

Acknowledgements

Appendix. Supplementary data

Supplementary data associated with this article can be found, in the online version, at doi:10.1016/j.neurobiolaging.2010.11.014.

References

Ashburner, J., Friston, K.J., 2000. Voxel-based morphometry—the methods. Neuroimage 11, 805–821.

Baddeley, A. D., Emslie, H., Nimmo-Smith, I., 1994. The Doors and People Test: A Test of Visual and Verbal Recall and Recognition. Bury St Edmunds, Flempton.

Bäckman, L., Andersson, J.L., Nyberg, L., Winblad, B., Nordberg, A., Almkvist, O., 1999. Brain regions associated with episodic retrieval in normal aging and Alzheimer's disease. Neurology 52, 1861–1870.

Bartzokis, G., 2004. Age-related myelin breakdown: a developmental model of cognitive decline and Alzheimer's disease. Neurobiol. Aging 25, 5–18.

Bartzokis, G., Lu, P.H., Mintz, J., 2007. Human brain myelination and amyloid beta deposition in Alzheimer's disease. Alzheimers Dement. 3, 122–125.

Bosma, G.P., Rood, M.J., Huizinga, T.W., de Jong, B.A., Bollen, E.L., van Buchem, M.A., 2000. Detection of cerebral involvement in patients with active neuropsychiatric systemic lupus erythematosus by the use of volumetric magnetization transfer imaging. Arthritis Rheum. 43, 2428–2436.

Bozzali, M., Franceschi, M., Falini, A., Pontesilli, S., Cercignani, M., Magnani, G., Scotti, G., Comi, G., Filippi, M., 2001. Quantification of tissue damage in AD using diffusion tensor and magnetization transfer MRI. Neurology 57, 1135–1137.

Braak, H., Braak, E., 1996. Development of Alzheimer-related neurofibrillary changes in the neocortex inversely recapitulates cortical myelogenesis. Acta Neuropathol. 92, 197–201.

Braak, H., Rüb, U., Schultz, C., Del Tredici, K., 2006. Vulnerability of cortical neurons to Alzheimer's and Parkinson's diseases. J. Alzheimers Dis. 9, 35–44.

Buckner, R.L., Snyder, A.Z., Shannon, B.J., LaRossa, G., Sachs, R., Fotenos, A.F., Sheline, Y.I., Klunk, W.E., Mathis, C.A., Morris, J.C., Mintun, M.A., 2005. Molecular, structural, and functional characterization of Alzheimer's disease: evidence for a relationship between default activity, amyloid, and memory. J. Neurosci. 25, 7709–7717.

Bussière, T., Gold, G., Kövari, E., Giannakopoulos, P., Bouras, C., Perl, D.P., Morrison, J.H., Hof, P.R., 2003. Stereologic analysis of neurofibrillary tangle formation in prefrontal cortex area 9 in aging and Alzheimer's disease. Neuroscience 117, 577–592.

Cabeza, R., Ciaramelli, E., Olson, I.R., Moscovitch, M., 2008. The parietal cortex and episodic memory: an attentional account. Nat. Rev. Neurosci. 9, 613–625.

Cabeza, R., Nyberg, L., 2000. Neural bases of learning and memory: functional neuroimaging evidence. Curr. Opin. Neurol. 13, 415–421.

Cercignani, M., Bozzali, M., Iannucci, G., Comi, G., Filippi, M., 2001. Magnetisation transfer ratio and mean diffusivity of normal appearing white and grey matter from patients with multiple sclerosis. J. Neurol. Neurosurg., Psychiatry 70, 311–317.

Chance, S.A., Casanova, M.F., Switala, A.E., Crow, T.J., 2006. Minicolumnar structure in Heschl's gyrus and planum temporale: Asymmetries in relation to sex and callosal fiber number. Neuroscience 143, 1041–1050.

Cohen, J., 1988. Statistical Power Analysis for the Behavioral Sciences, second ed. Lawrence Erlbaum Associates, Hillsdale, NJ, USA.

DePartz, M., Bilocq, V., De Wilde, V., Seron, X., Pillon, A., 2001. LEXIS—Tests pour le diagnostic des troubles lexicaux chez le patient aphasique. Solal, Marseille.

Desgranges, B., Baron, J.C., de la Sayette, V., Petit-Taboué, M.C., Benali, K., Landeau, B., Lechevalier, B., Eustache, F., 1998a. The neural substrates of memory systems impairment in Alzheimer's disease. A PET study of resting brain glucose utilization. Brain 121, 611–631.

Desgranges, B., Baron, J.C., Eustache, F, 1998b. The functional neuroanatomy of episodic memory: the role of the frontal lobes, the hippocampal formation, and other areas. Neuroimage 8, 198–213.

Duda, R.O., Hart, P.E., Stork, D.G., 2001. Pattern Classification. John Wiley & Sons, New York.

Duncan, J., Owen, A.M, 2000. Common regions of the human frontal lobe recruited by diverse cognitive demands. Trends Neurosci. 23, 475–483.

Duyckaerts, C., Delatour, B., Potier, M., 2009. Classification and basic pathology of Alzheimer disease. Acta Neuropathol. 118, 5–36.

Fellgiebel, A., Schermuly, I., Gerhard, A., Keller, I., Albrecht, J., Weibrich, C., Müller, M.J., Stoeter, P., 2008. Functional relevant loss of long association fibre tracts integrity in early Alzheimer's disease. Neuropsychologia 46, 1698–1706.

Fields, R.D., 2005. Myelination: an overlooked mechanism of synaptic plasticity? Neuroscientist 11, 528–531.

Fletcher, P.C., Shallice, T., Frith, C.D., Frackowiak, R.S., Dolan, R.J., 1998. The functional roles of prefrontal cortex in episodic memory. II. Retrieval. Brain 121, 1249–1256.

Folstein, M.F., Folstein, S.E., McHugh, P.R., 1975. "Mini-mental state". A practical method for grading the cognitive state of patients for the clinician. J. Psychiatr. Res. 12, 189–198.

Frisoni, G.B., Lorenzi, M., Caroli, A., Kemppainen, N., Någren, K., Rinne, J.O., 2009. In vivo mapping of amyloid toxicity in Alzheimer disease. Neurology 72, 1504–1511.

Frisoni, G.B., Pievani, M., Testa, C., Sabattoli, F., Bresciani, L., Bonetti, M., Beltramello, A., Hayashi, K.M., Toga, A.W., Thompson, P.M., 2007. The topography of grey matter involvement in early and late onset Alzheimer's disease. Brain 130, 720–730.

Grober, E., Buschke, H., 1987. Genuine memory deficits in dementia. Dev. Neuropsychol. 3, 13–36.

Grön, G., Bittner, D., Schmitz, B., Wunderlich, A.P., Riepe, M.W., 2002. Subjective memory complaints: objective neural markers in patients with Alzheimer's disease and major depressive disorder. Ann. Neurol. 51, 491–498.

Gunning-Dixon, F.M., Brickman, A.M., Cheng, J.C., Alexopoulos, G.S., 2009. Aging of cerebral white matter: a review of MRI findings. Int. J. Geriatr. Psychiatry 24, 109–117.

Hirono, N., Mori, E., Ishii, K., Imamura, T., Tanimukai, S., Kazui, H., Hashimoto, M., Takatsuki, Y., Kitagaki, H., Sasaki, M., 2001. Neuronal substrates for semantic memory: a positron emission tomography study in Alzheimer's disease. Dement. Geriatr. Cogn. Disord. 12, 15–21.

Holmes, C., Boche, D., Wilkinson, D., Yadegarfar, G., Hopkins, V., Bayer, A., Jones, R.W., Bullock, R., Love, S., Neal, J.W., Zotova, E., Nicoll, J.A., 2008. Long-term effects of Abeta42 immunisation in Alzheimer's disease: follow-up of a randomised, placebo-controlled phase I trial. Lancet. 372, 216–223.

Huang, J., Auchus, A.P., 2007. Diffusion tensor imaging of normal appearing white matter and its correlation with cognitive functioning in mild cognitive impairment and Alzheimer's disease. Ann. N. Y. Acad. Sci. 1097, 259–264.

Ishii, K., Kawachi, T., Sasaki, H., Kono, A.K., Fukuda, T., Kojima, Y., Mori, E., 2005. Voxel-based morphometric comparison between early- and late-onset mild Alzheimer's disease and assessment of diagnostic performance of z score images. AJNR Am. J. Neuroradiol. 26, 333–340.

Kabani, N.J., Sled, J.G., Chertkow, H., 2002. Magnetization transfer ratio in mild cognitive impairment and dementia of Alzheimer's type. Neuroimage 15, 604–610.

Kavcic, V., Ni, H., Zhu, T., Zhong, J., Duffy, C.J., 2008. White matter integrity linked to functional impairments in aging and early Alzheimer's disease. Alzheimers Dement. 4, 381–389.

Kim, H., Cabeza, R., 2009. Common and specific brain regions in high-versus low-confidence recognition memory. Brain Res. 1282, 103–113.

Kimura, F., Itami, C., 2009. Myelination and isochronicity in neural networks. Front. Neuroanat. 3, 12.

Kinney, H.C., Brody, B.A., Kloman, A.S., Gilles, F.H., 1988. Sequence of central nervous system myelination in human infancy. II. Patterns of myelination in autopsied infants. J. Neuropathol. Exp. Neurol. 47, 217–234.

Knyazeva, M.G., Jalili, M., Brioschi, A., Bourquin, I., Fornari, E., Hasler, M., Meuli, R., Maeder, P., Ghika, J., 2010. Topography of EEG multivariate phase synchronization in early Alzheimer's disease. Neurobiol. Aging 31, 1132–1144.

Liu, Y., Spulber, G., Lehtimäki, K.K., Könönen, M., Hallikainen, I., Gröhn, H., Kivipelto, M., Hallikainen, M., Vanninen, R., Soininen, H., 2009. Diffusion tensor imaging and Tract-Based Spatial Statistics in Alzheimer's disease and mild cognitive impairment. Neurobiol. Aging, doi:10.1016/j.neurobiolaging.2007.10.011.

Madden, D.J., Bennett, I.J., Song, A.W., 2009. Cerebral white matter integrity and cognitive aging: contributions from diffusion tensor imaging. Neuropsychol. Rev. 19, 415–435.

Maldjian, J.A., Laurienti, P.J., Kraft, R.A., Burdette, J.H., 2003. An automated method for neuroanatomic and cytoarchitectonic atlas-based interrogation of fMRI data sets. Neuroimage 19, 1233–1239.

Mattis, S., 1976. Mental status examination for organic mental syndrome in the elderly patient, in: Bellack, L., Karasu, T. (Eds.), Geriatric Psychiatry. Grune & Stratton, New York, pp. 77–121.

McKhann, G., Drachman, D., Folstein, M., Katzman, R., Price, D., Stadlan, E.M., 1984. Clinical diagnosis of Alzheimer's disease: report of the NINCDS-ADRDA Work Group under the auspices of Department of Health and Human Services Task Force on Alzheimer's Disease. Neurology 34, 939–944.

Medina, D., DeToledo-Morrell, L., Urresta, F., Gabrieli, J.D.E., Moseley, M., Fleischman, D., Bennett, D.A., Leurgans, S., Turner, D.A., Stebbins, G.T., 2006. White matter changes in mild cognitive impairment and AD: A diffusion tensor imaging study. Neurobiol. Aging 27, 663–672.

Morris, J.C., 1993. The Clinical Dementia Rating (CDR): current version and scoring rules. Neurology 43, 2412–2414.

Morrison, J.H., Hof, P.R., 2007. Life and death of neurons in the aging cerebral cortex. Int. Rev. Neurobiol. 81, 41–57.

Nakata, Y., Sato, N., Nemoto, K., Abe, O., Shikakura, S., Arima, K., Furuta, N., Uno, M., Hirai, S., Masutani, Y., Ohtomo, K., Barkovich, A.J., Aoki, S., 2009. Diffusion abnormality in the posterior cingulum and hippocampal volume: correlation with disease progression in Alzheimer's disease. Magn. Reson. Imaging 27, 347–354.

Nelson, P.T., Abner, E.L., Scheff, S.W., Schmitt, F.A., Kryscio, R.J., Jicha, G.A., Smith, C.D., Patel, E., Markesbery, W.R., 2009a. Alzheimer's-type neuropathology in the precuneus is not increased relative to other areas of neocortex across a range of cognitive impairment. Neurosci. Lett. 450, 336–339.

Nelson, P.T., Braak, H., Markesbery, W.R., 2009b. Neuropathology and cognitive impairment in Alzheimer disease: a complex but coherent relationship. J. Neuropathol. Exp. Neurol. 68, 1–14.

Oishi, K., Faria, A., Jiang, H., Li, X., Akhter, K., Zhang, J., Hsu, J.T., Miller, M.I., van Zijl, P.C.M., Albert, M., Lyketsos, C.G., Woods, R., Toga, A.W., Pike, G.B., Rosa-Neto, P., Evans, A., Mazziotta, J., Mori, S., 2009. Atlas-based whole brain white matter analysis using large deformation diffeomorphic metric mapping: application to normal elderly and Alzheimer's disease participants. Neuroimage 46, 486–499.

O'Sullivan, M., Jones, D.K., Summers, P.E., Morris, R.G., Williams, S.C., Markus, H.S., 2001. Evidence for cortical "disconnection" as a mechanism of age-related cognitive decline. Neurology 57, 632–638.

Parazzini, C., Baldoli, C., Scotti, G., Triulzi, F., 2002. Terminal zones of myelination: MR evaluation of children aged 20–40 months. AJNR Am. J. Neuroradiol. 23, 1669–1673.

Penhune, V.B., Zatorre, R.J., MacDonald, J.D., Evans, A.C., 1996. Inter-hemispheric anatomical differences in human primary auditory cortex: probabilistic mapping and volume measurement from magnetic resonance scans. Cereb. Cortex 6, 661–672.

Puel, M., Hugonot-Diener, L., 1996. Presenting by the GRECO group of the French adaptation of a cognitive assessment scale used in Alzhiemer type dementia. Presse Medicine 22, 1028–1132.

Rémy, F., Mirrashed, F., Campbell, B., Richter, W., 2005. Verbal episodic memory impairment in Alzheimer's disease: a combined structural and functional MRI study. Neuroimage 25, 253–266.

Rose, S.E., Janke, A.L., Chalk, J.B., 2008. Gray and white matter changes in Alzheimer's disease: a diffusion tensor imaging study. J. Magn. Reson. Imaging 27, 20–26.

Rovaris, M., Agosta, F., Sormani, M.P., Inglese, M., Martinelli, V., Comi, G., Filippi, M., 2003. Conventional and magnetization transfer MRI predictors of clinical multiple sclerosis evolution: a medium-term follow-up study. Brain 126, 2323–2332.

Schmidtke, K., Hüll, M., Talazko, J., 2005. Posterior cortical atrophy: variant of Alzheimer's disease? A case series with PET findings. J. Neurol. 252, 27–35.

Schuz, A., Braitenberg, V., 2002. The human cortical white matter: Quantitative aspects of cortico-cortical long-range connectivity, in: Schultz, A., Miller, R. (Eds.), Cortical Areas, Unity and Diversity. Conceptual Advances in Brain Research, London, pp. 377–386.

Sclan, S.G., Reisberg, B., 1992. Functional assessment staging (FAST) in Alzheimer's disease: reliability, validity, and ordinality. Int. Psychogeriatr. 4 suppl 1, 55–69.

Seldon, H.L., 1981. Structure of human auditory cortex. I. Cytoarchitectonics and dendritic distributions. Brain Res. 229, 277–294.

Semendeferi, K., Lu, A., Schenker, N., Damasio, H., 2002. Humans and great apes share a large frontal cortex. Nat. Neurosci. 5, 272–276.

Shin, J., Lee, S., Kim, S., Kim, Y., Cho, S., 2008. Multitracer PET imaging of amyloid plaques and neurofibrillary tangles in Alzheimer's disease. Neuroimage 43, 236–244.

Sormani, M.P., Iannucci, G., Rocca, M.A., Mastronardo, G., Cercignani, M., Minicucci, L., Filippi, M., 2000. Reproducibility of magnetization transfer ratio histogram-derived measures of the brain in healthy volunteers. AJNR Am. J. Neuroradiol. 21, 133–136.

Stahl, R., Dietrich, O., Teipel, S.J., Hampel, H., Reiser, M.F., Schoenberg, S.O., 2007. White matter damage in Alzheimer disease and mild cognitive impairment: assessment with diffusion-tensor MR imaging and parallel imaging techniques. Radiology 243, 483–492.

Stanisz, G.J., Kecojevic, A., Bronskill, M.J., Henkelman, R.M., 1999. Characterizing white matter with magnetization transfer and T. Magn. Reson. Med. 2, 42, 1128–1136.

Stebbins, G.T., Murphy, C.M., 2009. Diffusion tensor imaging in Alzheimer's disease and mild cognitive impairment. Behav. Neurol. 21, 39–49.

Stricker, N.H., Schweinsburg, B.C., Delano-Wood, L., Wierenga, C.E., Bangen, K.J., Haaland, K.Y., Frank, L.R., Salmon, D.P., Bondi, M.W., 2009. Decreased white matter integrity in late-myelinating fiber pathways in Alzheimer's disease supports retrogenesis. Neuroimage 45, 10–16.

Thompson, P.M., Hayashi, K.M., Dutton, R.A., Chiang, M., Leow, A.D., Sowell, E.R., De Zubicaray, G., Becker, J.T., Lopez, O.L., Aizenstein, H.J., Toga, A.W., 2007. Tracking Alzheimer's disease. Ann. N. Y. Acad. Sci. 1097, 183–214.

Tjoa, C.W., Benedict, R.H.B., Dwyer, M.G., Carone, D.A., Zivadinov, R., 2008. Regional specificity of magnetization transfer imaging in multiple sclerosis. J. Neuroimaging 18, 130–136.

Tulving, E., Kapur, S., Craik, F.I., Moscovitch, M., Houle, S., 1994. Hemispheric encoding/retrieval asymmetry in episodic memory: positron emission tomography findings. Proc. Natl. Acad. Sci. U. S. A. 91, 2016–2020.

Van Buchem, M.A., McGowan, J.C., Kolson, D.L., Polansky, M., Grossman, R.I., 1996. Quantitative volumetric magnetization transfer analysis in multiple sclerosis: estimation of macroscopic and microscopic disease burden. Magn. Reson. Med. 36, 632–636.

Van Es, A.C.G.M., van der Flier, W.M., Admiraal-Behloul, F., Olofsen, H., Bollen, E.L.E.M., Middelkoop, H.A.M., Weverling-Rijnsburger, A.W.E., van der Grond, J., Westendorp, R.G.J., van Buchem, M.A., 2007. Lobar distribution of changes in gray matter and white matter in memory clinic patients: detected using magnetization transfer imaging. AJNR Am. J. Neuroradiol. 28, 1938–1942.

Van Waesberghe, J.H., van Walderveen, M.A., Castelijns, J.A., Scheltens, P., Lycklamaà Nijeholt, G.J., Polman, C.H., Barkhof, F, 1998. Patterns of lesion development in multiple sclerosis: longitudinal observations with T1-weighted spin-echo and magnetization transfer MR. AJNR Am. J. Neuroradiol. 19, 675–683.

Van der Flier, W.M., van den Heuvel, D.M.J., Weverling-Rijnsburger, A.W.E., Bollen, E.L.E.M., Westendorp, R.G.J., van Buchem, M.A., Middelkoop, H.A.M., 2002. Magnetization transfer imaging in normal aging, mild cognitive impairment, and Alzheimer's disease. Ann. Neurol. 52, 62–67.

Vogt, B.A., Vogt, L.J., Vrana, K.E., Gioia, L., Meadows, R.S., Challa, V.R., Hof, P.R., Van Hoesen, G.W., 1998. Multivariate analysis of laminar patterns of neurodegeneration in posterior cingulate cortex in Alzheimer's disease. Exp. Neurol. 153, 8–22.

Warrier, C., Wong, P., Penhune, V., Zatorre, R., Parrish, T., Abrams, D., Kraus, N., 2009. Relating structure to function: Heschl's gyrus and acoustic processing. J. Neurosci. 29, 61–69.

Wen, W., Sachdev, P., 2004. The topography of white matter hyperintensities on brain MRI in healthy 60 to 64-year-old individuals. Neuroimage 22, 144–154.

Yakovlev, P., Lecours, A., 1967. The myelogenetic cycles of regional maturation of the rain. In: Minkowski, A. (ed). Regional Development of the Brain in Early Life. Blackwell Scientific Publications, Boston, MA, USA. p. 3–70.

Yoshiura, T., Mihara, F., Ogomori, K., Tanaka, A., Kaneko, K., Masuda, K., 2002. Diffusion tensor in posterior cingulate gyrus: correlation with cognitive decline in Alzheimer's disease. Neuroreport 13, 2299–2302.

Zahn, R., Garrard, P., Talazko, J., Gondan, M., Bubrowski, P., Juengling, F., Slawik, H., Dykierek, P., Koester, B., Hull, M., 2006. Patterns of regional brain hypometabolism associated with knowledge of semantic features and categories in Alzheimer's disease. J. Cogn. Neurosci. 18, 2138–2151.